Title

Sulfated Cellulose Nanofibrils from Chlorosulfonic Acid Treatment and Their Wet Spinning into High-Strength Fibers

Journal

Biomacromolecules, 23(3)

ISSN

1525-7797

Authors

Pingrey, Benjamin
Hsieh, You-Lo

Publication Date

2022-03-14

DOI

10.1021/acs.biomac.1c01505

Peer reviewed

pubs.acs.org/Biomac

Article

Sulfated Cellulose Nanofibrils from Chlorosulfonic Acid Treatment and Their Wet Spinning into High-Strength Fibers

Benjamin Pingrey and You-Lo Hsieh*

Cite This: https://doi.org/10.1021/acs.biomac.1c01505

Read Online

ACCESS | Metrics & More | Article Recommendations | Supporting Information

ABSTRACT: This paper presents the proof of concept for a facile sulfation-disintegration approach toward generating sulfated cellulose nanofibrils (SCNF) via direct sulfation of rice straw cellulose with chlorosulfonic acid (HSO_3Cl) followed by blending. The direct sulfation of cellulose with chlorosulfonic acid (HSO_3Cl) was optimized at acid ratios of 1−1.5 HSO_3Cl per anhydroglucose unit (AGU) and short reaction times (30−60 min) at ambient temperature to produce SCNF with tunable charges of 1.0−2.2 mmol/g, all in impressively high yields of 94−97%. SCNF were characterized via AFM, TEM, FTIR, and XRD. SCNF lengths (L: 0.75−1.24 μm) and widths (W: 3.9−5.9 nm) decreased with harsher sulfation, while heights (H: 1.23−1.32 nm) remained relatively static. The SCNF had uniquely anisotropic cross sections (W/H: 3.0−4.7) and high aspect ratios (L/H: 568−984) while also exhibiting amphiphilicity, thixotropy, and shear thinning behaviors that closely followed a power law model. Aqueous SCNF dispersions could be wet spun into organic and mixed organic/ionic coagulants, producing continuous fibers possessing an impressively high tensile strength and Young's modulus of up to 675 ± 120 MPa and 26 ± 5 GPa, respectively.

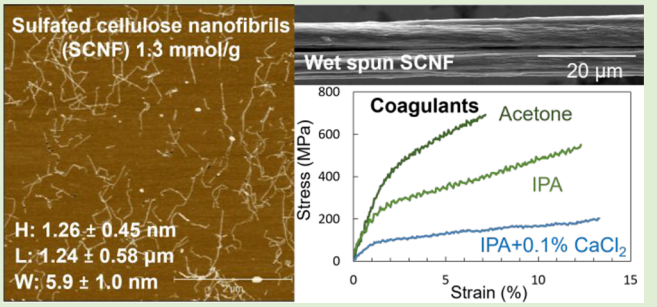

INTRODUCTION

Cellulose, the most abundant biopolymer on the planet,[1] has been widely utilized in its native fibrous forms in textiles and paper for millennia. For over a century, dissolved and derivatized cellulose has also enabled processing into fibers and films for additional products and uses. In these cases, the cellulose I crystalline structure is lost and replaced with the cellulose II crystalline structure, a change which is accompanied by a loss in mechanical strength.[2] Nanocelluloses contain crystalline domains isolated from native cellulose without dissolution and therefore retain the cellulose I crystalline structure and possess remarkable mechanical properties. For instance, hydrolysis by concentrated sulfuric acid removes amorphous cellulose chains, leaving highly crystalline rod-like cellulose nanocrystals (CNCs) that have a tensile strength and Young's modulus as high as 7.5 GPa and ∼150 GPa, respectively,[3] but in low yields. Toward the other extreme, intense mechanical means can produce thinner and longer cellulose nanofibrils (CNF) in higher yields. To reduce the mechanical energy needed to separate cellulose into CNF, chemical pretreatments are often performed. Among the most reported is the regioselective oxidation of cellulose mediated by the aminoxyl radical (2,2,6,6-tetramethylpiperidin-1-yl)oxyl (TEMPO) followed by mechanical disintegration to produce carboxylated CNF. TEMPO-oxidized CNF (TCNF) can be produced in near-total yields and are highly dispersible in aqueous media, making them attractive for a myriad of applications including gas membranes, packaging materials, composites, aerogels, superabsorbent materials, biomedical scaffolds, printed electronics, and energy storage devices.[4−7]

As is the case for any nanomaterial, translating the ultrahigh mechanical strength of nanocelluloses into macroscopic structures remains a significant engineering challenge. For fiber formation, the high aspect ratios and specific surfaces of CNF provide advantages over CNCs. However, aligning CNF during processing is challenging yet critical for the bulk materials to inherit the longitudinal strength of the nanofibrils. A proven process for effective alignment of long chain polymers, such as dissolved cellulose and cellulose derivatives, to produce fibers is wet spinning. In wet spinning, the dissolved polymer is extruded into a coagulation bath containing an antisolvent, which causes the polymer to fall out of solution and solidify into a continuous filament. In fact, wet spinning of both TCNF[8−15] and unmodified[16,17] CNF has been demonstrated and reviewed.[18−20] For wet spinning CNF, the most reported coagulants have included acetone,[8−11,16,21] ethanol,[11,14,17] THF,[14,15] and dioxane.[14] Aqueous calcium chloride solutions have also been utilized as coagulants for

Received: November 17, 2021
Revised: January 25, 2022

TCNF,[11−13] with multivalent Ca^{2+} ions screening electrostatic repulsion among the carboxylated nanofibrils to induce aggregation and ionic cross-linking.

High-strength fibers have been engineered based on the principles of aligning ultrahigh molecular weight and/or structurally rigid polymers; the intrinsically high crystallinity and aspect ratios of CNF meet both criteria, making them promising candidates. To advance nanocelluloses into fibers, scalable reactions and engineering processes must be considered. Additional routes to CNF beyond TEMPO are desirable not only to alleviate the high cost of the reagent but also to expand the diversity of available surface chemistries. Sulfation, while well-established for dissolving cellulose to produce regenerated cellulose, is a less-explored alternative to produce anionic CNF. A variety of sulfating agents have been applied to cellulose. Chlorosulfonic acid, which reacts readily with alcohols to give the corresponding alkyl sulfates, has been used to produce water-soluble cellulose sulfates.[22,23] Performed under milder conditions, reacting nanocelluloses with chlorosulfonic acid has been shown to add sulfate half-ester groups to CNCs produced from sulfuric acid hydrolysis[24] and CNF produced by homogenization,[25] giving respective charges of 0.4 and 0.56−1.79 mmol/g. Sulfonated CNF has also been produced by a two-step reaction involving the periodate cleavage of cellulose's 2,3 vicinal diol to produce 2,3-dialdehyde cellulose, followed by reaction with bisulfite and homogenization to a 91% yield with 0.51 mmol/g of hydroxy sulfonate groups.[26] Using a deep eutectic solvent of sulfamic acid and urea at 150 °C in conjunction with microfluidization has also produced 4.4 nm wide sulfated CNF with 1.44−3.00 mmol/g sulfate contents.[27] However, a possible carbamation side reaction may complicate this process by generating other unintended functional groups. Regardless of the reactions, processes, and cellulose feedstock involved, sulfated cellulose or nanocellulose variants have typically been lauded for their aqueous solubility, dispersibility, and superior absorbent properties imparted by the introduction of hygroscopic sulfate groups.[22,28,29] Thus far, sulfated CNF has not been exploited for more diverse functional applications, particularly those building upon the unique intrinsic strength and anisotropy of CNF.

This study sought to quantify the effectiveness of chlorosulfonic acid treatment for simultaneously pretreating and functionalizing cellulose to produce sulfated CNF (SCNF) while also demonstrating the potential of SCNF as a structural material by wet spinning them into high-strength fibers. Cellulose was heterogeneously sulfated with chlorosulfonic acid in anhydrous *N*,*N*-dimethylformamide, with reaction conditions being optimized to minimize dissolution while providing sufficient sulfation to facilitate disintegration into aqueous-dispersible SCNF through high-speed blending. The degree of sulfation was investigated by varying the stoichiometric ratio of chlorosulfonic acid per anhydroglucose unit (AGU) and the reaction time at ambient temperature. Structure−property relationships were explored between SCNF charge, dimensions, morphology, and rheology. Aqueous SCNF dispersions were wet spun into varied coagulants of acetone, isopropanol, and mixtures of calcium chloride and isopropanol to explore the assembly of SCNF into fibers and relate SCNF charge and spinning conditions to fiber morphology and strength.

EXPERIMENTAL SECTION

Materials. Sodium hydroxide (NaOH, 97.0%), toluene (99.9%), hydrochloric acid (HCl, 1.0 M), and Dowex Marathon C (H-form) acidic ion-exchange resin beads were obtained from Fisher Scientific. Reagent grade ethanol, calcium chloride ($CaCl_2$, 99%), potassium bromide (KBr, 99%), and anhydrous *N*,*N*-dimethylformamide (DMF) were obtained from Sigma-Aldrich. Chlorosulfonic acid (HSO_3Cl, 99%), toluene (99.5%), and sodium chlorite ($NaClO_2$, 80% purity) were obtained from Alfa Aesar. Potassium hydroxide (KOH, 85%) was obtained from Acros. Reagent grade isopropanol (IPA) and acetone were obtained from Spectrum Chemical. Purified water was obtained from a Milli-Q Advantage A10 water purification system. All dialysis steps were performed by using regenerated cellulose dialysis tubing with a nominal molecular weight cutoff of 12−14 kDa from Fisher Scientific. All chemicals were used as received without further purification. Cellulose was isolated from Calrose variety rice straw by using a previously reported procedure;[30] dewaxing by Soxhlet extraction with a 2:1 v/v mixture of refluxing toluene/ethanol, delignification with 1.4 wt % acidified NaClO, and hemicellulose removal with 5 wt % KOH.

Sulfation of Cellulose via Chlorosulfonic Acid. Cellulose and all glassware used were oven-dried prior to use to eliminate moisture. For a typical sulfation run, 0.5 g of cellulose was placed in a stoppered 50 mL Erlenmeyer flask, to which 22 mL of anhydrous DMF was added. The mixture was allowed to stir vigorously for a period of ∼10 min to allow the cellulose to disperse. Chlorosulfonic acid in varied quantities of 0.10−0.31 mL, or 0.5−1.5 HSO_3Cl per anhydroglucose unit (AGU) molar ratios, was added dropwise to 3 mL of anhydrous DMF chilled in an ice bath. This HSO_3Cl/DMF mixture was then added to cellulose/DMF to begin the reaction. All reactions were performed at ambient temperature (25 °C) for 30−60 min. Termination was performed by the addition of 10 mL of purified water. The sulfated cellulose was centrifuged and washed with purified water. The remaining acid and DMF were removed through dialysis against purified water for ∼7 days until no change in the conductivity of the water was observed.

Defibrillation into SCNF. Following dialysis, the sulfated cellulose was dispersed at a concentration of 0.2 wt % in 250 mL of purified water and blended at 30000 rpm in a high-speed blender (Vitamix 5200) for a total of 30 min in 5 min increments to avoid overheating. The aqueous suspension was then centrifuged (Eppendorf 5804R, 5000 rpm, 15 min) to separate out large fragments that did not defibrillate. A known volume of supernatant and the precipitate were oven-dried in tared vessels to determine their mass and concentration, respectively. The wt % of the product that remained dispersed in the supernatant relative to the original sulfated cellulose was reported as the SCNF yield.

SCNF Characterization. The height and length of SCNF were determined through atomic force microscopy (AFM) (Asylum Research MFP-3D) by using OMCL-AC160TS standard silicon probes (nominal tip radius of 7 nm, spring constant of 26 N/m). Several drops of diluted SCNF dispersion (ca. 0.0001 wt %) were deposited on freshly cleaved mica discs and allowed to dry. Surface profiles were collected in tapping mode under ambient conditions and processed by using the open-source software programs Gwyddion and ImageJ to derive the fibril heights and lengths. For height determination 140+ fibrils were measured while for length 100+ were used, spread across multiple AFM images. Aggregates, where individual fibers could not be differentiated, were excluded from length analysis.

SCNF widths were determined by using transmission electron microscopy (TEM) (JEOL JSM-1230). Samples were prepared by placing a drop of diluted SCNF dispersion (ca. 0.0001 wt %) on a glow-discharged carbon grid and blotting away the excess after 10 min. Samples were negatively stained with 2 wt % uranyl acetate to enhance contrast. Micrographs were taken with a LaB_6 electron source by using an accelerating voltage of 100 kV. Analysis was performed by using ImageJ.

https://doi.org/10.1021/acs.biomac.1c01505
Biomacromolecules XXXX, XXX, XXX−XXX

Scheme 1. Generation of SCNF from Cellulose through Reaction with Chlorosulfonic Acid Followed by High-Speed Blending

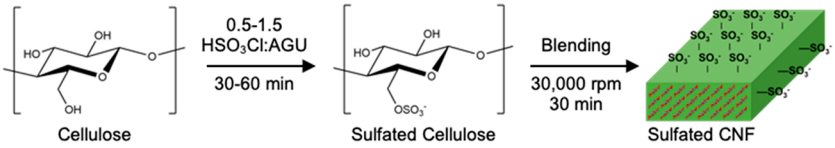

The surface charges of SCNF samples were determined by conductometric titration. To obtain pristine CNF for titration, aliquots of SCNF were dialyzed against purified water for several days to remove small-molecule contaminants. They were then run through an ion-exchange column packed with an acidic ion-exchange resin (Dowex Marathon C, H-form) that exchanges metallic cations for protons to ensure the sulfate half-ester groups on the SCNF were in their acid forms. The SCNF samples (50 mL, diluted to ca. 0.05 wt %) were titrated with 0.01 M sodium hydroxide while measuring the conductivity by with a pH meter (Oakton pH/CON 510). A representative titration curve is provided in the Supporting Information (Figure S1).

Fourier transform infrared spectroscopy (FTIR) was performed by using a Thermo-Nicolet 6700 infrared spectrometer. Aqueous SCNF samples were freeze-dried and then mixed with ground potassium bromide and pressed into pellets. Spectra were collected in transmittance mode from an accumulation of 64 scans at a resolution of 2 cm^{-1} over the range 4000−400 cm^{-1}.

X-ray powder diffraction was performed on a Bruker D8 Advance Eco diffractometer with a Cu Kα X-ray source. Powdered cellulose and air-dried SCNF samples were scanned at 2θ values ranging from 5° to 40° with an angular increment of 0.015° and a scan time of 0.5 s per increment. The crystallinity of cellulose samples was estimated by using both the Segal method[31,32] and a peak deconvolution using four crystalline peaks and the fitting software Fityk.[32] Voigt functions were used to model the shape of XRD peaks.

Aqueous SCNF Dispersion Properties. The surface tensions of SCNF dispersions were measured on a Kruss K100 tensiometer by using the Wilhelmy plate method. The viscosities of aqueous SCNF dispersions were measured by using a Brookfield DV3T rheometer with a concentric cylinder geometry. Samples of SCNF with charges of 1.3, 1.8, and 2.2 mmol/g were degassed for several seconds in a bath sonicator (Branson 2510) prior to analysis. Viscosity measurements were taken at 25 °C in a water bath at concentrations from 0.3 to 0.6 wt % and shear rates from 0.1 to 100 s^{-1}.

Wet Spinning of SCNF. Aqueous dispersions of 1.3 and 1.8 mmol/g SCNF were concentrated to 0.65 wt % by using a rotary evaporator. Aqueous SCNF spin dope was dispensed via a syringe pump fitted with a 27 gauge needle with 210 μm inner diameter (ID) and its tip submerged in a 60 cm long horizontal channel filled with a coagulant of either acetone, IPA, or IPA with 0.1 wt % $CaCl_2$. The extrusion rate, controlled via syringe pump, was approximately 144 cm/min (3 mL/h). After moving through the coagulation bath, fibers were pulled through an air gap to dry before being wound onto a cylindrical collector driven by a DC motor at a rate of ∼170 cm/min.

The diameter, tensile strength, and Young's modulus of wet-spun fibers were determined by using a Zellweger-Uster Mantis single fiber tensile tester designed for testing cotton fibers.[33] Fibers were conditioned at 21 °C and 65% relative humidity for at least 24 h prior to tensile tests. SEM images of wet-spun fibers were taken on a Thermo Fisher Quattro S Environmental SEM. Fibers were sputtered with ∼1.5 nm of gold prior to imaging. Optical microscopy images of fibers were taken under crossed polars with the fiber angled at 45° with respect to the polarization plane.

RESULTS AND DISCUSSION

Functionalization and Disintegration of Cellulose into SCNF. Heterogeneous sulfation of cellulose with chlorosulfonic acid (HSO_3Cl) proceeds via bimolecular substitution, and the repulsive charge induced by sulfation helps facilitate the disintegration of sulfated cellulose by high-speed blending into aqueously dispersible SCNF (Scheme 1). Because of the complete solubility of cellulose sulfates at higher degrees of substitution, the success of this approach hinges on identifying reaction conditions that minimize dissolution while providing sufficient sulfation to disintegrate macroscale sulfated cellulose into SCNF. Sulfation of cellulose with HSO_3Cl has been shown to exhibit many characteristics typical of S_N2 reactions, such as selectivity for primary hydroxyls over secondary and tertiary sites;[34] it is similar to TEMPO oxidation in that regard.

By varying the HSO_3Cl/AGU molar ratio from 0.5 to 1.5 for reaction times of 30 to 60 min, sulfated celluloses with charges ranging from 0.45 ± 0.10 to 2.20 ± 0.10 mmol/g were produced (Figure 1a). The HSO_3Cl/AGU ratio was found to be the most significant determiner of charge, with a lesser effect observed for reaction time over the conditions studied. The skew in the 30 and 60 min trendlines indicates a two-factor interaction between time and HSO_3Cl/AGU ratio, wherein longer reaction times magnify the effect of the HSO_3Cl/AGU ratio.

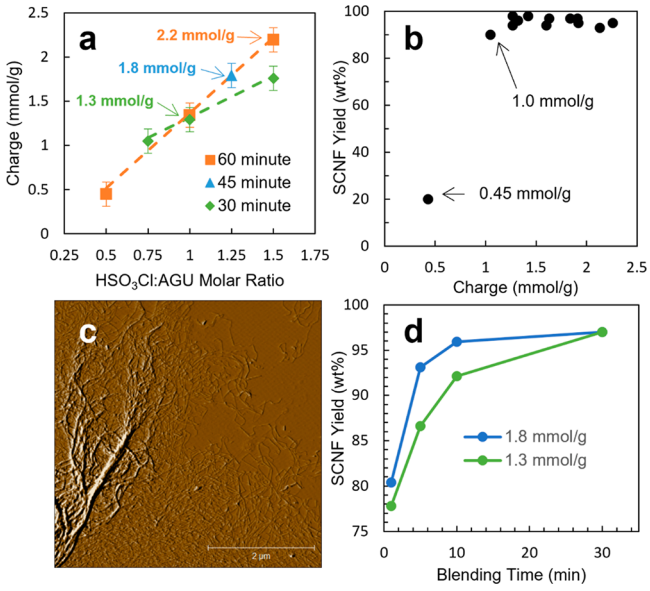

Figure 1. Effect of sulfation reaction conditions followed by high-speed blending (30K rpm, 30 min): (a) surface charge as a function of HSO_3Cl/AGU molar ratio and reaction time; (b) SCNF yield as a function of surface charge (30 min blending); (c) SCNF with a charge of 1.0 mmol/g, showing some branching fibrils; (d) SCNF yield as a function of blending time.

High-speed blending of rice straw cellulose without any pretreatment, even for an extended period of 60 min, has been shown to yield less than 5% nanofibrils.[35] Under all reaction conditions tested, blending of sulfated cellulose for 30 min dramatically increased nanofibril yields. The lowest yield of 20% SCNF corresponds to sulfated cellulose with the lowest

https://doi.org/10.1021/acs.biomac.1c01505
Biomacromolecules XXXX, XXX, XXX−XXX

charge, 0.45 mmol/g, produced with a 0.5 HSO_3Cl/AGU and 60 min reaction time (Figure 1b). Sulfated cellulose produced under all other reaction conditions could be defibrillated into SCNF and dispersed in the supernatants at high 90−97% yields (see all yield and charge data in Table S1). AFM of 1.0 mmol/g SCNF (0.75 HSO_3Cl/AGU, 30 min) showed some highly branched and entangled fibrillar structures (Figure 1c) which were not observed under any other conditions. This observation, along with the 90% yield, indicates 1.0 mmol/g to be just below the sulfation threshold required to permit full disintegration of macroscale sulfated cellulose into nanoscale SCNF.

While a blending time of 30 min was chosen for the sake of direct comparison with previously reported TCNF from the same feedstock and defibrillation conditions,[36] shorter blending proved to still be effective at liberating large amounts of SCNF, with 1.3 mmol/g SCNF (1 HSO_3Cl/AGU, 30 min) and 1.8 mmol/g showing yields of 78% and 80%, respectively, after only 1 min of blending. These yields are significantly higher than that of rice straw 1.29 mmol/g TCNF at the same blending time (ca. 50%[36]), showcasing the impressive effectiveness of sulfation as a pretreatment for producing nanofibrils.

Morphology and Characterization of SCNF. From the seven reactions studied, i.e., different HSO_3Cl/AGU ratios and reaction times, three high-yielding SCNF representing three charge levels of 1.3 mmol/g (1.0 HSO_3Cl/AGU, 30 min), 1.8 mmol/g (1.25 HSO_3Cl/AGU, 45 min), and 2.2 mmol/g (1.5 HSO_3Cl/AGU, 60 min) were selected for further analysis. The average SCNF length (L) decreased from 1.24 to 1.08 μm and 0.75 μm with increasing levels of sulfation from 1.3 mmol/g to 1.8 and 2.2 mmol/g (Figure 2a−c). A progressive reduction in

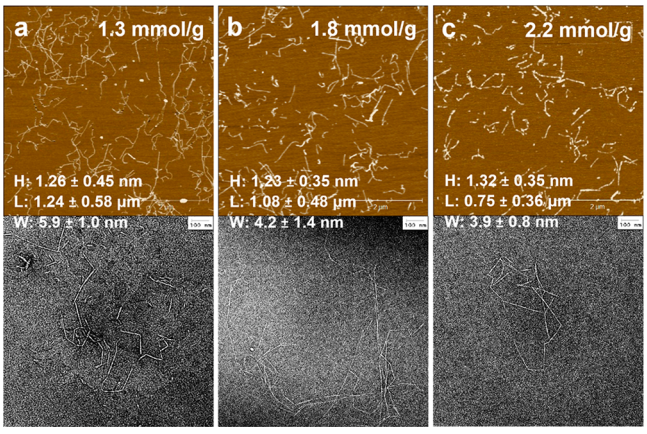

Figure 2. Characterization of SCNF: (a−c) AFM (top) and TEM (bottom) micrographs of SCNF with 1.3, 1.8, and 2.2 mmol/g charges. Dimensions presented as value ± standard deviation.

fibril width (W) from 5.9 nm to 4.2 and 3.9 nm was also observed with increasing sulfation. The height (H) values of all SCNF ranged from 1.23 to 1.32 nm, with little variation between reaction conditions. Most distinctively, the L/H aspect ratios of all three SCNF were very high, though they showed a downward trend from 984 to 843 and 568 with increasing sulfation. Based on the H values from AFM and W values from TEM, all three SCNF had rectangular cross sections, with W/H ratios of 3.0−4.7. The low H values could be in part attributed to the tendency of AFM to underrepresent the heights of nanoscale features, sometimes attributed to sample deformation by the tip,[37] the presence of salts or other deposits on the substrate surface,[38] or when the lateral dimensions being measured are smaller than the effective size of the tip,[39] as is the case here. However, these effects are unlikely to account for the significant cross-sectional anisotropy observed. TEMPO CNF produced from the same cellulose feedstock and bearing similar charge (1.29 mmol/g) showed a much more isotropic cross section (W: 2.09 nm; H: 1.52 nm),[36] indicating that the anisotropic rectangular cross section is associated with the chlorosulfonic acid reaction and not related to cellulose source. Despite the morphological differences, the high 94−97% yields for SCNF were similar to the 96.8% yield of TCNF, also disintegrated by the same blending, affirming that the sulfation of cellulose by chlorosulfonic acid is robust and highly effective at producing SCNF over a wide range of charges.

FTIR transmittance spectra of SCNF samples show all major peaks characteristic of cellulose: broad OH stretching around 3500 cm^{-1}, CH_2 stretching at 2900 cm^{-1}, and C−O−C stretching of the β-1,4-glycosidic linkage at 898 cm^{-1} (Figure 3a). In addition, two new peaks characteristic of sulfate half-ester groups appeared at 811 and 1230 cm^{-1} that can be attributed to the S−O and S═O stretching vibrations, respectively. While the intensity of these two sulfate ester peaks showed no clear trend with the levels of sulfation, the water scissoring peak at 1641 cm^{-1} intensified in all three SCNF. This intensification could be attributed to an increase in hygroscopicity brought about by sulfation and has been observed previously for cellulose sulfates.[23] The most charged 2.2 mmol/g SCNF also showed sharpening of the OH stretching peak and a decrease in the prominence of the CH_2 stretching peak compared to the less sulfated SCNF. Both of these traits are more characteristic of amorphous celluloses,[40] indicating possible reduction in crystallinity brought about by the harshest reaction conditions.

XRD profiles of rice straw cellulose as well as 1.3 and 1.8 mmol/g SCNF further support the notion that chlorosulfonic acid treatment reduces cellulose crystallinity (Figure 3b). The Segal method for calculating cellulose crystallinities gave values of 70%, 50%, and 40% for cellulose, 1.3 mmol/g SCNF, and 1.8 mmol/g SCNF, respectively. Peak deconvolution instead gave values of 76%, 67%, and 60%. Nanomaterials often show broadened peaks in XRD compared to their macroscopic counterparts as a result of the finite size of crystallites; this effect can be clearly seen in the XRD profiles for SCNF by the overlapping of the (200), (110), and ($1\bar{1}0$) peaks. The Segal method does not account for the broadening of crystalline peaks and as a result is expected to overestimate the amount of amorphous cellulose present. Consistently, both methods of analysis point to a progressive reduction in crystallinity with more sulfated SCNF. As CNF produced by blending the same starting cellulose alone showed slightly higher crystallinity,[35] the reduced crystallinity of SCNF was attributed mainly to the extent of sulfation. Nevertheless, both SCNF retained significant crystallinity.

All SCNF dispersions exhibited thixotropy. To account for this, viscosity measurements were taken after steady state was established for each shear rate. SCNF dispersions exhibited shear thinning behavior between shear rates of 0.1 and 100 s^{-1} (Figure 4a) that fit well to power law kinetics (Table S2). The viscosity of the most highly charged 2.2 mmol/g SCNF was approximately an order of magnitude below the 1.3 and 1.8 mmol/g SCNF at most shear rates tested. The significantly

https://doi.org/10.1021/acs.biomac.1c01505
Biomacromolecules XXXX, XXX, XXX−XXX

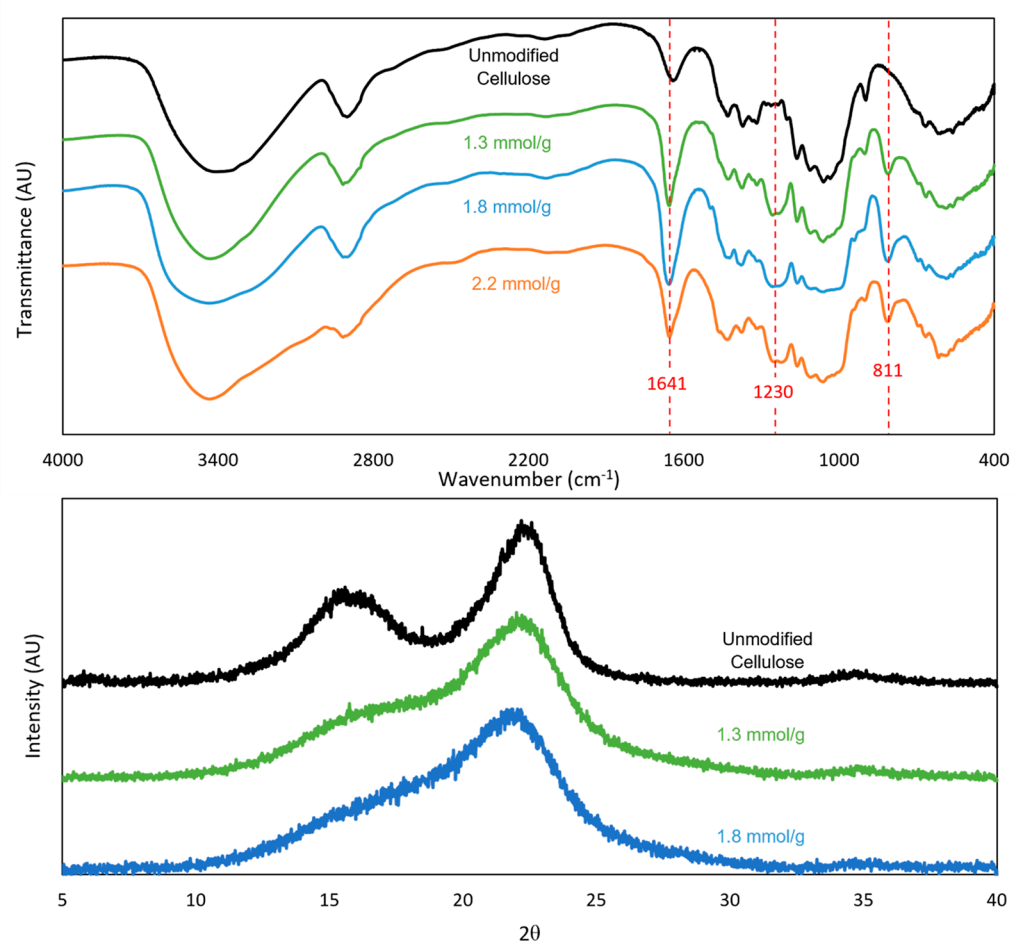

Figure 3. FTIR spectra (a) and XRD profiles (b) of selected SCNF samples and rice straw cellulose.

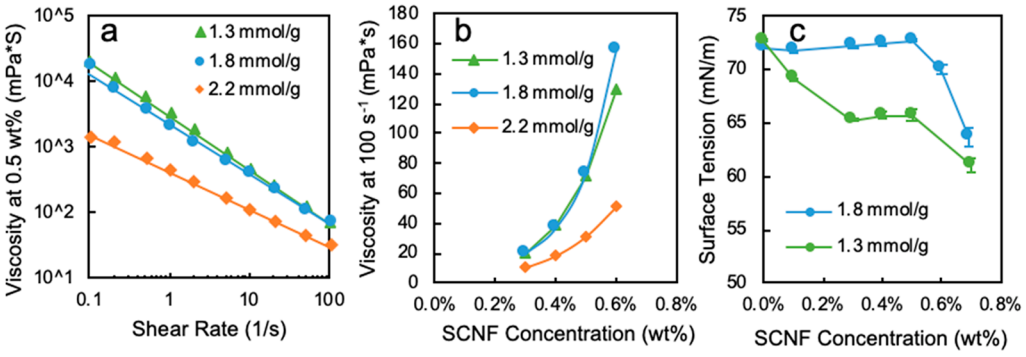

Figure 4. Aqueous SCH properties: (a) effective viscosities as a function of shear rate; (b) viscosities as a function of concentration; (c) surface tension as a function of concentration.

lower viscosity of the 2.2 mmol/g SCNF may be attributed to both reduced nanofibril lengths as well as higher charge, leading to increased electrostatic repulsion between fibrils and decreased propensity for entanglement. The thixotropic and shear thinning behaviors of SCNF are similar to those observed for TCNF.[36,41] At 0.5 wt %, the viscosities of the aqueous 1.3 mmol/g SCNF dispersions are similar to those reported for SCNF produced from softwood pulp by using sulfamic acid and urea,[27] indicating similarity in nanofibrillar characteristics between the two sulfation schemes. Aqueous SCNF also showed amphiphilicity, reducing the surface tension of water with increasing concentrations (Figure 4c). This reduction was more pronounced for higher anisotropic cross section (W/H: 4.7) and lower 1.3 mmol/g charged SCNF as compared to the less anisotropic (W/H: 3.4) and higher charged 1.8 mmol/g SCNF, which only showed a reduction at higher concentrations of 0.6−0.7%. This surface active behavior of the 1.8 mmol/g SCNF is once again, similar to TCNF, which exhibited a similar reduction in surface tension with 1.29 mmol/g charge at ca. 0.3%.[42] However, amphiphilicity of these SCNF has not been reported on any other sulfated or sulfonated nanocelluloses.

SCNF Cross Section and Surface Functionalization. Because of the semicrystalline structure of cellulose, only the

https://doi.org/10.1021/acs.biomac.1c01505
Biomacromolecules XXXX, XXX, XXX−XXX

chains in the amorphous regions or on exposed crystallite surfaces were susceptible to functionalization. Representing the degree of substitution (DS) on a basis of total anhydroglucose units in cellulose, therefore, does not reflect the surface characteristics of SCNF. To represent the functionalization of cellulose in terms of accessible surface hydroxyls, a model was developed based on cross-sectional dimensions determined by AFM and TEM. The model assumes that SCNF possess crystalline cores of the cellulose 1β structure with exposed hydrophilic (110) and (1$\bar{1}$0) planes bearing hydroxyl groups that are susceptible to chemical modification (Figure 5). The lattice parameters used for cellulose 1β are $\alpha = \beta = 90°$, $\gamma = 96.5°$, $a = 7.78$ Å, $b = 8.20$ Å, and $c = 10.38$ Å.[43]

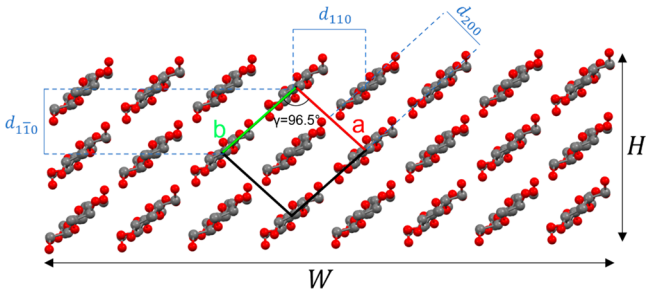

Figure 5. Cross-sectional model of SCNF with cellulose 1β unit cell and d-spacings indicated.

In this cross-sectional lattice, the number of chains in the width and height directions can be represented by $H/d_{1\bar{1}0} + 1$ and $W/d_{110} + 1$, where H and W are the fibril height and width as determined from AFM and TEM, respectively. The total number of cellulose chains in the cross section, N, is given by

$$N = \left(\frac{H}{d_{1\bar{1}0}} + 1\right)\left(\frac{W}{d_{110}} + 1\right)$$

The number of cellulose chains on the fibril surface along the (110) and (1$\bar{1}$0) planes, N_s, is expressed as

$$N_s = 2\left[\left(\frac{H}{d_{1\bar{1}0}} + 1\right) + \left(\frac{W}{d_{110}} + 1\right)\right] - 2 = 2\left(\frac{W+H}{5.65\ \text{Å}} + 1\right)$$

where the −2 is necessary to avoid double counting the corner chains and $d_{110} = d_{1\bar{1}0} = 5.65$ Å. The number of surface hydroxyls or OHs per AGU (φ) can be expressed by dividing the number of surface cellulose chains N_s by the total number of cellulose chains N and multiplying by the number of surface hydroxyls per exposed surface AGU, 1.5 (three surface hydroxyls—C2, C3, and C6—for every cellobiose or two AGU exposed on the 110 or 1$\bar{1}$0 planes).

$$\varphi = \frac{1.5N_s}{N} = \frac{3\left(\frac{W+H}{5.65\ \text{Å}} + 1\right)}{\left(\frac{W}{5.65\ \text{Å}} + 1\right)\left(\frac{H}{5.65\ \text{Å}} + 1\right)}$$

Finally, the percentage of exposed hydroxyls that are sulfated is expressed by dividing the charge (mmol/g) by the total AGU (mmol/g) multiplied φ as follows:

$$\%\ \text{exposed OH sulfated} = \frac{\text{SCNF charge}}{\text{total AGU}\cdot\varphi}$$

This fraction is shown alongside overall degree of substitution for SCNF samples in Table 1.

Table 1. Functionalization of SCNF Surface Hydroxyls

SCNF charge (mmol/g)	deg of substitution[a]	% exposed OH sulfated	% exposed C6 sulfated
1.3	0.24	19	57
1.8	0.34	24	72
2.2	0.43	31	93

[a]Number of sulfate groups per total AGU.

Previous work by using NMR on dissolved cellulose sulfate produced by the same reaction but under harsher conditions (2 HSO_3Cl/AGU for 5 h) found no measurable secondary C2/C3 hydroxyl substitution.[34] Because the reaction conditions used for this study were milder those cited above, it is reasonable to assume that C6 sulfation was dominant. That being the case, complete sulfation of exposed surface C6 hydroxyls is expected at 33% surface sulfation; the 2.2 mmol/g SCNF approaches this value at 31%, with an estimated 93% of accessible C6 hydroxyls sulfated. The simplicity and selectivity of chlorosulfonic acid treatment of cellulose under relatively mild conditions are particularly compelling in the context of competing with carboxylated TEMPO CNF, which is lauded for its specificity for C6 carboxylation.

Wet Spinning of SCNF. Aqueous SCNF with 1.3 and 1.8 mmol/g charges was wet-spun at 0.65 wt % concentration through a 27 gauge needle (210 μm ID). The extrusion and take-up rates were 144 and 170 cm/s, respectively, giving effective viscosities during extrusion on the order of 100 mPa·s. The prospect of higher spinning rate is promising by increasing the size of the coagulation batch to maintain adequate residence time as part of scaling up the wet spinning operation in the future. Several different coagulants were used, including acetone and IPA as organic coagulants and a mixed ionic/organic coagulant consisting of 0.1 wt % $CaCl_2$ in IPA. The removal of water from fibers coagulated in aqueous $CaCl_2$ necessitates a long and continuous coagulation path and long drying times that are difficult to implement on the laboratory scale. Using solutions of $CaCl_2$ in IPA alleviates this problem, with the increased volatility of isopropanol facilitating faster drying.

The spinnability of aqueous SCNF was found to vary with respect to their charges. The 1.3 mmol/g SCNF could be continuously spun into fibers in all coagulants tested. Under the same spinning conditions, the higher charged 1.8 mmol/g SCNF did not coagulate uniformly in either IPA or acetone, becoming fragmented or too delicate to be handled or collected. The poorer coagulation behavior of the 1.8 mmol/g SCNF in organic solvents may be attributed to several factors. The higher charge of the SCNF leads to increased interfibrillar electrostatic double-layer repulsion, hampering their association during coagulation. The higher quantities of hygroscopic sulfate groups in the 1.8 mmol/g SCNF also retain more bound water molecules, further hindering interfibrillar association and slowing coagulation. Conversely, the 1.8 mmol/g SCNF could be easily spun into IPA with 0.1 wt % $CaCl_2$. With divalent calcium ions screening electrostatic repulsion and higher charge facilitating ionic cross-linking, this system is well suited for spinning fibers from this more highly substituted SCNF.

Microscopy on wet-spun fibers showed clear evidence of nanofibrillar alignment, necessary for achieving strong fibers. Surface striations along the fibrillar axis were observed in SEM images (Figure 6a–d). Optical microscopy of fibers viewed

https://doi.org/10.1021/acs.biomac.1c01505
Biomacromolecules XXXX, XXX, XXX−XXX

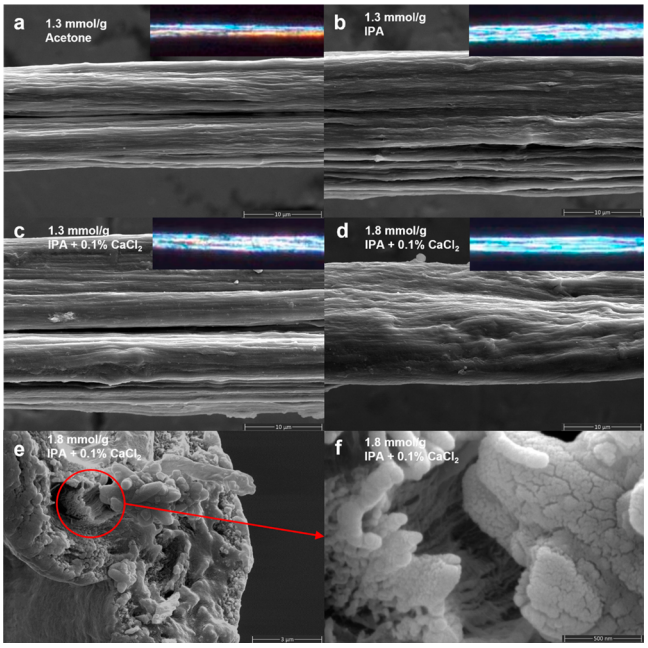

Figure 6. SEM of wet-spun SCNF fibers: (a–d) longitudinal images with charges and coagulants indicated; (e, f) fractured surface of SCNF in (d). Insets in (a–d): optical microscopy under crossed polars.

under crossed polars showed bright birefringence in all cases (Figure 6a–d, insets), further confirming alignment of SCNF in the bulk. SEM of a tensile fractured end from a fiber coagulated in $CaCl_2$/IPA showed lamellar structures aligned along the fibrillar axis (Figure 6e,f). While these oriented fibrillar structures showed clear SCNF alignment or assembly at the nanofibril level, interfibrillar spacings were also visible. Combined with the larger diameter of the fiber coagulated in $CaCl_2$/IPA, ionic coagulation of the more highly charged 1.8 mmol/g SCNF produced fibers with a greater degree of porosity than those 1.3 mmol/g charged SCNF coagulated in pristine organic solvents. The fibers coagulated in IPA and IPA + $CaCl_2$ also showed increased porosity as compared to those coagulated in acetone, as evidenced by the larger fiber diameter for equal spinning/take-up rates.

The tensile properties of the wet-spun SCNF fibers showed a strong dependence on the type of coagulant. The highest Young's modulus of 26.0 ± 4.8 GPa and tensile strength of 675 ± 120 MPa as well as the lowest breaking strain of 6.6 ± 1.2% were achieved for 1.3 mmol/g SCNF coagulated in acetone, followed by those coagulated in IPA and IPA/$CaCl_2$ with respective mean tensile modulus of 16.1 and 8.5 GPa and tensile strength of 422 and 188 MPa (Table 2).

The mechanical performance of wet-spun SCNF fibers was found to positively correlate with the relative speeds at which each solvent system is expected to coagulate (Figure 7a). Coagulation in acetone was visibly faster than in IPA, possibly due to the weaker interactions between acetone and SCNF; acetone cannot act as a hydrogen bond donor while IPA can. The IPA/$CaCl_2$ system coagulated even more slowly, as the ionic cross-linking and coagulating of the fiber's surface forming a skin that hampers ion diffusion to and from the core and water diffusion out of the fiber. This may also contribute to the increased porosity observed in fibers coagulated from the IPA/$CaCl_2$ system. The fibers spun from 1.8 mmol/g SCNF were equal in diameter and similar in tensile strength and modulus (ca. 219 MPa and 9 GPa, respectively) to those from 1.3 mmol/g SCNF, both spun into IPA/$CaCl_2$, but significantly lower strain at break.

When compared to fibers wet-spun from a variety of CNF—both TEMPO[8−16,20] and unmodified[16,17,20]—in the literature (Figure 7b), all four fibers from SCNF showed higher tensile strength at corresponding modulus, with the acetone coagulated fiber from 1.3 mmol/g SCNF having the highest tensile strength (675 ± 120 MPa) and modulus (26.0 ± 4.8 GPa) (Table S3). Only two previously reported fibers had higher modulus,[12,15] but their tensile strengths were lower than the highest in this study. Those reported fibers compared were mostly spun under similar conditions as the SCNF fibers reported here and coagulated predominantly in acetone or aqueous $CaCl_2$ with no polymeric additives. The TCNF charges reported were mostly between 0.54 and 0.65 mmol/g, with only three possessing higher charges of 1.36 mmol/g[16,21] and 1.5 mmol/g,[9] generally lower than the 1.3–1.8 mmol/g SCNF fibers. The fibers wet-spun from SCNF in acetone are among the strongest fibers wet-spun from CNF—either unmodified or TEMPO oxidized—without using flow focusing. In fact, all four fibers from SCNF were wet-spun without any additional drawing nor postspinning treatment to enhance orientation—highlighting the intrinsic attributes of SCNF as a structural material.

Given that one significant draw of nanocelluloses is their renewability, it is important to consider the sustainability and environmental impact of the chlorosulfonic acid/DMF system for producing SCNF compared to alternative routes. While anhydrous DMF makes the sulfation of cellulose robust and efficient, the impact of DMF may be minimized by reuse and recycling. The heterogeneous nature of this process makes collection of the macroscale cellulose sulfate product easy by simple solid–liquid separation processes of sedimentation and filtration. Because of the low concentration of chlorosulfonic acid in the reaction mixture (~1% v/v), additional acid could be readily added to the separated solvent for direct reuse. Built-up reaction byproducts (i.e., HCl) could be removed along with other impurities through a small purge stream.

CONCLUSIONS

This paper reports for the first time the facile sulfation-disintegration approach of producing sulfated CNF (SCNF)

Table 2. Properties of Wet-Spun SCNF Fibers[a]

SCNF charge (mmol/g)	coagulant	fiber diameter (μm)	strain at break (%)	tensile strength (MPa)	Young's modulus (GPa)
1.3	acetone	10.1 ± 1.2	6.6 ± 1.2	675 ± 120	26.0 ± 4.8
1.3	IPA	15.2 ± 3.0	8.4 ± 1.1	422 ± 160	16.1 ± 6.1
1.3	IPA + 0.1% $CaCl_2$	16.3 ± 2.4	12.6 ± 1.6	188 ± 53	8.5 ± 2.5
1.8	IPA + 0.1% $CaCl_2$	16.4 ± 3.6	7.0 ± 2.5	219 ± 60	9.3 ± 2.3

[a]All fibers were spun at 0.05 mL/min from a 27 gauge needle (ID = 210 μm) with a 0.65 wt % spinning dope.

https://doi.org/10.1021/acs.biomac.1c01505
Biomacromolecules XXXX, XXX, XXX–XXX

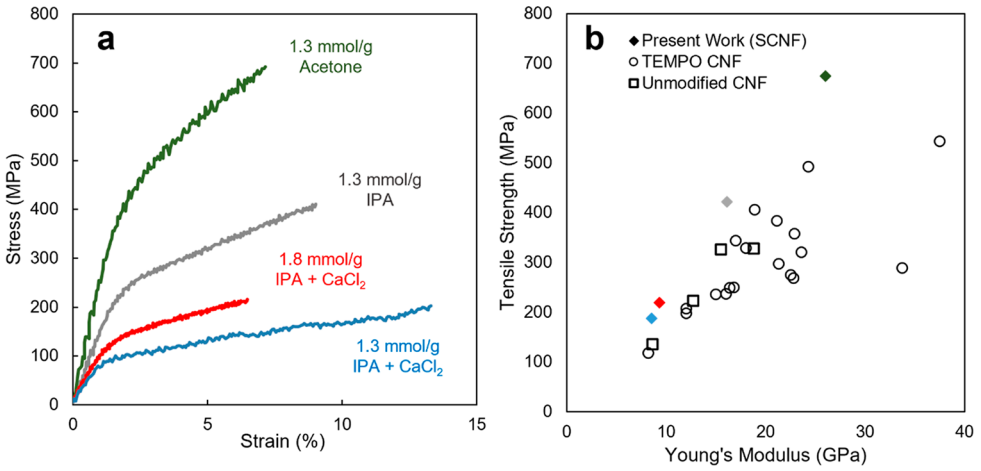

Figure 7. Tensile strength of wet-spun SCNF fibers: (a) representative stress−strain curves; (b) comparison of with other wet-spun CNF fibers in the literature.

by direct sulfation of macroscale cellulose with chlorosulfonic acid (HSO_3Cl) to achieve a tunable range of sulfation while avoiding dissolution. Robust sulfation at moderate 1 to 1.5 HSO_3Cl/AGU molar ratios at ambient temperature for 30−60 min produced sulfated cellulose that could be disintegrated by high-speed blending (30K rpm, 30 min) to yield 94−97% SCNF with 1.3−2.2 mmol/g charges. With increasing extent of sulfation, the resulting SCNF had similar heights (H) of 1.23−1.32 nm but lowered widths (W) from 5.9 to 3.9 nm and lengths (L) from 1.24 to 0.75 μm. All SCNF had anisotropic cross sections (W/H: 3.0−4.7) and very high aspect ratios (L/H: 568−984) as well as exhibited amphiphilic, thixotropic, and shear thinning behaviors between 0.1 and 100 s^{-1} shear rates. Aqueous SCNF with 1.3 and 1.8 mmol/g charges could be wet-spun into 10−16 μm wide fibers continuously without drawing. The strongest fibers were wet-spun from 1.3 mmol/g SCNF into acetone coagulant, achieving 26.0 GPa Young's modulus and 675 MPa tensile strength, the highest from wet-spinning of CNF, unmodified[16,17] or TEMPO oxidized,[8−15,21] without the use of flow focusing.

The application and product development of nanocelluloses are contingent upon the development of synthesis techniques that are robust and scalable while also providing a diverse range of surface chemistries. By applying an already established sulfation chemistry for industrial production of alkyl sulfates and soluble cellulose sulfates, this direct sulfation-disintegration scheme provides a scalable and lower cost alternative to TEMPO oxoammonium catalysts. While effort continues in advancing this promising approach to generate SCNF, high-strength fibers, and applications of both SCNF and fibers, this proof of concept advances the goal of bringing nanocellulose beyond the benchtop.

■ ASSOCIATED CONTENT

Supporting Information

The Supporting Information is available free of charge at https://pubs.acs.org/doi/10.1021/acs.biomac.1c01505.

Representative conductometric titration curve for determining charge; yield and charge data from all reaction conditions; power law viscosity fitting coefficients for SCNF dispersions; CNF and tensile properties of wet-spun fibers from the literature and this work (PDF)

■ AUTHOR INFORMATION

Corresponding Author

You-Lo Hsieh − *Biological and Agricultural Engineering, Chemical Engineering, University of California, Davis, Davis, California 95616, United States;* orcid.org/0000-0003-4795-260X; Phone: +1 530 752 0843; Email: ylhsieh@ucdavis.edu

Author

Benjamin Pingrey − *Biological and Agricultural Engineering, Chemical Engineering, University of California, Davis, Davis, California 95616, United States*

Complete contact information is available at: https://pubs.acs.org/10.1021/acs.biomac.1c01505

Notes

The authors declare no competing financial interest.

■ ACKNOWLEDGMENTS

The authors thank the California Rice Research Board (RU-9), the American Association of Textile Chemists and Colorists Foundation, and the United States Department of Defense's Science, Mathematics, and Research for Transformation (SMART) scholarship program for their respective financial support. The Thermo Fisher Quattro ESEM was also funded through the US National Science Foundation under Award DMR-1725618.

■ REFERENCES

(1) Habibi, Y.; Lucia, L. A.; Rojas, O. J. Cellulose Nanocrystals: Chemistry, Self-Assembly, and Applications. *Chem. Rev.* **2010**, *110* (6), 3479−3500.

(2) Nishino, T.; Takano, K.; Nakamae, K. Elastic Modulus of the Crystalline Regions of Cellulose Polymorphs. *J. Polym. Sci., Part B: Polym. Phys.* **1995**, *33* (11), 1647−1651.

(3) Moon, R. J.; Martini, A.; Nairn, J.; Simonsen, J.; Youngblood, J. Cellulose Nanomaterials Review: Structure, Properties and Nanocomposites. *Chem. Soc. Rev.* **2011**, *40* (7), 3941−3994.

(4) Stark, N. M. Opportunities for Cellulose Nanomaterials in Packaging Films: A Review and Future Trends. *J. Renewable Mater.* **2016**, *4* (5), 313−326.

(5) Wang, Q.; Yao, Q.; Liu, J.; Sun, J.; Zhu, Q.; Chen, H. Processing Nanocellulose to Bulk Materials: A Review. *Cellulose* **2019**, *26* (13), 7585−7617.

(6) Thomas, B.; Raj, M. C.; Athira, B. K.; Rubiyah, H. M.; Joy, J.; Moores, A.; Drisko, G. L.; Sanchez, C. Nanocellulose, a Versatile Green Platform: From Biosources to Materials and Their Applications. *Chem. Rev.* **2018**, *118* (24), 11575−11625.
(7) Abitbol, T.; Rivkin, A.; Cao, Y.; Nevo, Y.; Abraham, E.; Ben-Shalom, T.; Lapidot, S.; Shoseyov, O. Nanocellulose, a Tiny Fiber with Huge Applications. *Curr. Opin. Biotechnol.* **2016**, *39*, 76−88.
(8) Iwamoto, S.; Isogai, A.; Iwata, T. Structure and Mechanical Properties of Wet-Spun Fibers Made from Natural Cellulose Nanofibers. *Biomacromolecules* **2011**, *12* (3), 831−836.
(9) Geng, L.; Chen, B.; Peng, X.; Kuang, T. Strength and Modulus Improvement of Wet-Spun Cellulose I Filaments by Sequential Physical and Chemical Cross-Linking. *Mater. Des.* **2017**, *136*, 45−53.
(10) Yao, J.; Chen, S.; Chen, Y.; Wang, B.; Pei, Q.; Wang, H. Macrofibers with High Mechanical Performance Based on Aligned Bacterial Cellulose Nanofibers. *ACS Appl. Mater. Interfaces* **2017**, *9* (24), 20330−20339.
(11) Wang, L.; Lundahl, M. J.; Greca, L. G.; Papageorgiou, A. C.; Borghei, M.; Rojas, O. J. Effects of Non-Solvents and Electrolytes on the Formation and Properties of Cellulose I Filaments. *Sci. Rep.* **2019**, *9* (1), 1−11.
(12) Kim, H. C.; Kim, D.; Lee, J. Y.; Zhai, L.; Kim, J. Effect of Wet Spinning and Stretching to Enhance Mechanical Properties of Cellulose Nanofiber Filament. *Int. J. Pr. Eng. Man.- GT.* **2019**, *6* (3), 567−575.
(13) Kafy, A.; Kim, H. C.; Zhai, L.; Kim, J. W.; Hai, L. V.; Kang, T. J.; Kim, J. Cellulose Long Fibers Fabricated from Cellulose Nanofibers and Its Strong and Tough Characteristics. *Sci. Rep.* **2017**, *7* (1), 1−8.
(14) Walther, A.; Timonen, J. V. I.; Díez, I.; Laukkanen, A.; Ikkala, O. Multifunctional High-Performance Biofibers Based on Wet-Extrusion of Renewable Native Cellulose Nanofibrils. *Adv. Mater.* **2011**, *23* (26), 2924−2928.
(15) Torres-Rendon, J. G.; Schacher, F. H.; Ifuku, S.; Walther, A. Mechanical Performance of Macrofibers of Cellulose and Chitin Nanofibrils Aligned by Wet-Stretching: A Critical Comparison. *Biomacromolecules* **2014**, *15* (7), 2709−2717.
(16) Lundahl, M. J.; Cunha, A. G.; Rojo, E.; Papageorgiou, A. C.; Rautkari, L.; Arboleda, J. C.; Rojas, O. J. Strength and Water Interactions of Cellulose i Filaments Wet-Spun from Cellulose Nanofibril Hydrogels. *Sci. Rep.* **2016**, *6* (1), 1−13.
(17) Mohammadi, P.; Toivonen, M. S.; Ikkala, O.; Wagermaier, W.; Linder, M. B. Aligning Cellulose Nanofibril Dispersions for Tougher Fibers. *Sci. Rep.* **2017**, *7* (1), 1−10.
(18) Lundahl, M. J.; Klar, V.; Wang, L.; Ago, M.; Rojas, O. J. Spinning of Cellulose Nanofibrils into Filaments: A Review. *Ind. Eng. Chem. Res.* **2017**, *56* (1), 8−19.
(19) Clemons, C. Nanocellulose in Spun Continuous Fibers: A Review and Future Outlook. *J. Renewable Mater.* **2016**, *4* (5), 327−339.
(20) Rosén, T.; Hsiao, B. S.; Söderberg, L. D. Elucidating the Opportunities and Challenges for Nanocellulose Spinning. *Adv. Mater.* **2021**, *33* (28), 2001238.
(21) Vuoriluoto, M.; Orelma, H.; Lundahl, M.; Borghei, M.; Rojas, O. J. Filaments with Affinity Binding and Wet Strength Can Be Achieved by Spinning Bifunctional Cellulose Nanofibrils. *Biomacromolecules* **2017**, *18* (6), 1803−1813.
(22) Shet, R. T.; Raj, R.; Wallajapet, P. Sulfonated Cellulose Having Improved Absorbent Properties. US5703225A, 1995.
(23) Horikawa, M.; Fujiki, T.; Shirosaki, T.; Ryu, N.; Sakurai, H.; Nagaoka, S.; Ihara, H. The Development of a Highly Conductive PEDOT System by Doping with Partially Crystalline Sulfated Cellulose and Its Electric Conductivity. *J. Mater. Chem. C* **2015**, *3* (34), 8881−8887.
(24) Lin, N.; Dufresne, A. Surface Chemistry, Morphological Analysis and Properties of Cellulose Nanocrystals with Gradiented Sulfation Degrees. *Nanoscale* **2014**, *6* (10), 5384−5393.
(25) Luo, J.; Semenikhin, N.; Chang, H.; Moon, R. J.; Kumar, S. Post-Sulfonation of Cellulose Nanofibrils with a One-Step Reaction to Improve Dispersibility. *Carbohydr. Polym.* **2018**, *181*, 247−255.
(26) Liimatainen, H.; Visanko, M.; Sirviö, J.; Hormi, O.; Niinimäki, J. Sulfonated Cellulose Nanofibrils Obtained from Wood Pulp through Regioselective Oxidative Bisulfite Pre-Treatment. *Cellulose* **2013**, *20* (2), 741−749.
(27) Sirviö, J. A.; Ukkola, J.; Liimatainen, H. Direct Sulfation of Cellulose Fibers Using a Reactive Deep Eutectic Solvent to Produce Highly Charged Cellulose Nanofibers. *Cellulose* **2019**, *26* (4), 2303−2316.
(28) Zhang, J.; Jiang, N.; Dang, Z.; Elder, T. J.; Ragauskas, A. J. Oxidation and Sulfonation of Cellulosics. *Cellulose* **2008**, *15* (3), 489−496.
(29) Hou, Q. X.; Liu, W.; Liu, Z. H.; Bai, L. L. Characteristics of Wood Cellulose Fibers Treated with Periodate and Bisulfite. *Ind. Eng. Chem. Res.* **2007**, *46* (23), 7830−7837.
(30) Lu, P.; Hsieh, Y.-L. Preparation and Characterization of Cellulose Nanocrystals from Rice Straw. *Carbohydr. Polym.* **2012**, *87* (1), 564−573.
(31) Segal, L.; Creely, J. J.; Martin, A. E.; Conrad, C. M. An Empirical Method for Estimating the Degree of Crystallinity of Native Cellulose Using the X-Ray Diffractometer. *Text. Res. J.* **1959**, *29* (10), 786−794.
(32) Park, S.; Baker, J. O.; Himmel, M. E.; Parilla, P. A.; Johnson, D. K. Cellulose Crystallinity Index: Measurement Techniques and Their Impact on Interpreting Cellulase Performance. *Biotechnol. Biofuels* **2010**, *3* (1), 1−10.
(33) Hsieh, Y. -L; Hu, X. P.; Wang, A. Single Fiber Strength Variations of Developing Cotton Fibers—Strength and Structure of G. Hirsutum and G. Barbedense. *Text. Res. J.* **2000**, *70* (8), 682−690.
(34) Zhang, K.; Brendler, E.; Geissler, A.; Fischer, S. Synthesis and Spectroscopic Analysis of Cellulose Sulfates with Regulable Total Degrees of Substitution and Sulfation Patterns via 13C NMR and FT Raman Spectroscopy. *Polymer* **2011**, *52* (1), 26−32.
(35) Jiang, F.; Hsieh, Y.-L. Chemically and Mechanically Isolated Nanocellulose and Their Self-Assembled Structures. *Carbohydr. Polym.* **2013**, *95* (1), 32−40.
(36) Jiang, F.; Han, S.; Hsieh, Y.-L. Controlled Defibrillation of Rice Straw Cellulose and Self-Assembly of Cellulose Nanofibrils into Highly Crystalline Fibrous Materials. *RSC Adv.* **2013**, *3* (30), 12366−12375.
(37) García, R.; Pérez, R. Dynamic Atomic Force Microscopy Methods. *Surf. Sci. Rep.* **2002**, *47* (6−8), 197−301.
(38) Moreno-Herrero, F.; Colchero, J.; Baró, A. M. DNA Height in Scanning Force Microscopy. *Ultramicroscopy* **2003**, *96* (2), 167−174.
(39) Santos, S.; Barcons, V.; Christenson, H. K.; Font, J.; Thomson, N. H. The Intrinsic Resolution Limit in the Atomic Force Microscope: Implications for Heights of Nano-Scale Features. *PLoS One* **2011**, *6* (8), e23821.
(40) Ciolacu, D.; Ciolacu, F.; Popa, V. I. Amorphous Cellulose—Structure and Characterization. *Cellul. Chem. Technol.* **2011**, *45* (1−2), 13−21.
(41) Lasseuguette, E.; Roux, D.; Nishiyama, Y. Rheological Properties of Microfibrillar Suspension of TEMPO-Oxidized Pulp. *Cellulose* **2008**, *15* (3), 425−433.
(42) Xu, X.; Hsieh, Y.-L. Aqueous Exfoliated Graphene by Amphiphilic Nanocellulose and Its Application in Moisture-Responsive Foldable Actuators. *Nanoscale* **2019**, *11* (24), 11719−11729.
(43) Nishiyama, Y.; Langan, P.; Chanzy, H. Crystal Structure and Hydrogen-Bonding System in Cellulose Iβ from Synchrotron X-Ray and Neutron Fiber Diffraction. *J. Am. Chem. Soc.* **2002**, *124* (31), 9074−9082.

https://doi.org/10.1021/acs.biomac.1c01505
Biomacromolecules XXXX, XXX, XXX−XXX